

# Thin film dynamics in a liquid lined circular pipe

Roberto Camassa

Long Lee

*Department of Mathematics*

*University of North Carolina at Chapel Hill*

*Chapel Hill, NC 27599*

May 2, 2005

## **Abstract**

A two-phase core annular flow in a cylindrical pipe is considered. The inner core is assumed to be a pressure driven gas flow. The other phase is highly viscous fluid lining the inner wall of the pipe. Several models are presented, including the classic Poiseuille solution for two-phase flows, to predict the mean thickness of the liquid layer in the experiment by Kim et al. (1986), where a given fixed gas-flow rate drags the liquid injected into the pipe at a fixed feed rate. In particular, a nonlinear evolution equation based on the lubrication approximation is derived. The strong pressure-driven gas flow is incorporated as a forcing term into the equation for the liquid, with an effective viscosity for turbulent flow replacing the molecular viscosity of the gas. We study numerically the interface evolution of an initially axisymmetric disturbance of the annular film of viscous liquid. The mean height of the liquid layer in the experiment can be accurately predicted using this model, and the existence of the ring-like waves reported in the experiments is confirmed by the interfacial dynamics of the model.

## **1 Problem formulation and Poiseuille solutions**

Kim, Greene, Sankaran, and M. A. Sackner [5] conducted an experiment to investigate the effects of air drag in the dynamics of the mucus layer that coats the airways of human respiratory systems. The schematic diagram of the experiment is shown as in Figure 1(a). A pair of identical glass tubes in series are connected via a cylindrical chamber. Liquid is forced at a fixed rate into an annular space formed between the chamber and the tube walls. The liquid is then carried away along the wall of the upper tube by an airflow that continuously passes upward through the tubes. When the liquid layer reaches the top of the upper tube, it is allowed to overflow naturally into the collection cup. Analysis of such a two-layer gas-liquid flow

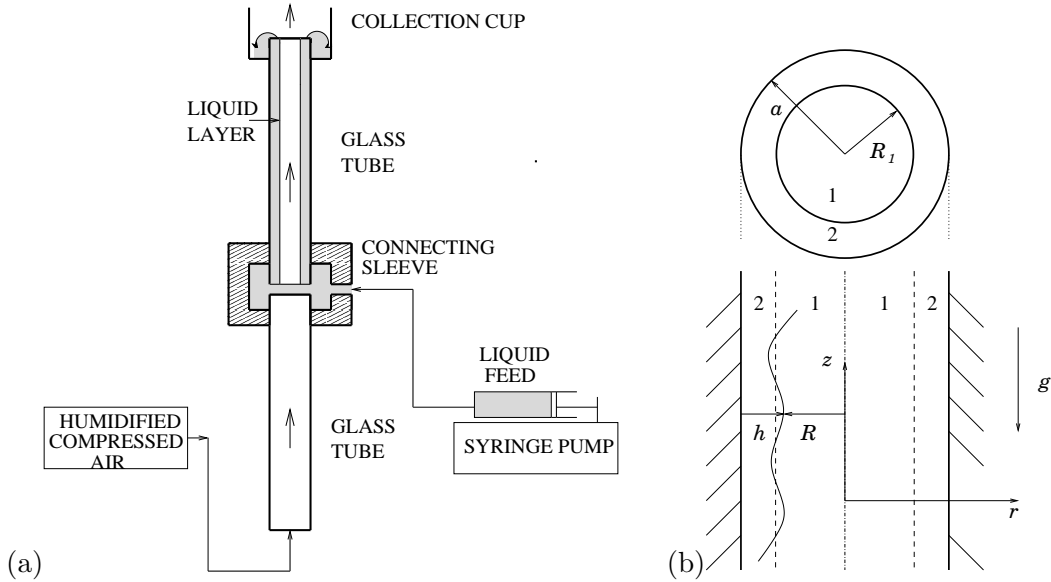


Figure 1: (a) Schematic diagram of experimental system of Kim et al. [5]. (b) The geometry of the concentric two-phase flow system.

within a tube is important for understanding the mobility of thin layers of biofluid in wetted membranes, especially when the core flow is a high-Reynolds-number, (strong) pressure driven gas flow. We remark that Kim et al. [5] actually considered several fluids with viscoelastic properties, in addition to Newtonian fluids of same viscosity which were used as control. In this paper we consider the Newtonian case only.

Assuming axisymmetry for either the liquid or the gas mean flow, the incompressible Navier-Stokes equations in cylindrical coordinates govern the dynamics of both fluids,

$$\begin{aligned}
 \rho(u_t + uu_z + wu_r) &= -p_z + \mu \left( \frac{1}{r} \partial_r (r u_r) + u_{zz} \right) - g, \\
 \rho(w_t + uw_z + ww_r) &= -p_r + \mu \left( \frac{1}{r} \partial_r (r w_r) + w_{zz} - \frac{w}{r^2} \right), \\
 \frac{1}{r} \partial_r (r w) + u_z &= 0,
 \end{aligned} \tag{1}$$

where the coordinates are  $(z, \theta, r)$ , with associated velocity components  $(u, v, w)$ . Here  $p$  is pressure,  $\rho$  is density,  $\mu$  is molecular viscosity, and  $g$  is gravity. For a flat interface, the boundary and interfacial conditions are: (i) no-slip boundary condition at the wall, (ii) the continuity of velocity across the interface, (iii) the continuity of normal and tangential stress across the interface. In searching for the Poiseuille solutions for this system, the only nonzero velocity component is the axial velocity  $u$ , which is a function depending solely on  $r$ . Let the axial velocity for the gas be  $u^{(g)}$ , and let the liquid velocity be  $u^{(l)}$ . The radius of the pipe is  $r = a$ , and the interface is located at  $r = R$ . While applying conditions (i) - (iii) to

equations (1), the axial velocity for each layer is

$$\begin{aligned} u^{(g)}(r) &= -\frac{G^{(g)}}{4\nu^{(g)}}(R^2 - r^2) - \frac{G^{(l)}}{4\nu^{(l)}}(a^2 - R^2) + \frac{R^2 g}{2\mu^{(l)}} \log(a/R)(\rho^{(l)} - \rho^{(g)}), \\ u^{(l)}(r) &= -\frac{G^{(l)}}{4\nu^{(l)}}(a^2 - r^2) + \frac{R^2 g}{2\mu^{(l)}} \log(a/r)(\rho^{(l)} - \rho^{(g)}), \end{aligned} \quad (2)$$

where  $\nu^{(\cdot)}$  is kinematic viscosity and  $G^{(g)}$  is defined by

$$G^{(g)} = \frac{1}{\rho^{(g)}} \frac{\partial p^{(g)}}{\partial z} + g. \quad (3)$$

The relation between  $G^{(g)}$  and  $G^{(l)}$  is

$$\rho^{(l)} G^{(l)} - \rho^{(g)} G^{(g)} = g(\rho^{(l)} - \rho^{(g)}). \quad (4)$$

The gas flux can be obtained from the velocity  $u^{(g)}$ ,

$$\begin{aligned} Q^{(g)} &= \int_0^R 2\pi u^{(g)}(r) r dr \\ &= -\frac{\pi G^{(g)}}{8\nu^{(g)}} R^4 - \frac{\pi G^{(l)}}{4\nu^{(l)}} (a^2 R^2 - R^4) + \frac{\pi R^4 g}{2\mu^{(l)}} \log(a/R)(\rho^{(l)} - \rho^{(g)}). \end{aligned} \quad (5)$$

Similarly the liquid flux is

$$\begin{aligned} Q^{(l)} &= \int_R^a 2\pi u^{(l)}(r) r dr \\ &= -\frac{\pi G^{(l)}}{8\nu^{(l)}} (a^2 - R^2)^2 + \frac{\pi R^2 g}{2\mu^{(l)}} \left[ \frac{1}{2}(a^2 - R^2) - a^2 \log(a/R) \right] (\rho^{(l)} - \rho^{(g)}). \end{aligned} \quad (6)$$

Given the fluxes  $Q^{(g)}$ ,  $Q^{(l)}$ , the three equations (4), (5), and (6) can be solved together for the three unknowns  $G^{(g)}$ ,  $G^{(l)}$ , and  $R$ . The theoretical prediction for the liquid layer thickness is then given by the difference  $a - R$ .

## 1.1 Comparison with experimental data

In order to compare with the experimental data, the parameters used in the Poiseuille solutions are as follows: the density of air is  $1.205 \times 10^{-3}$  g/ml<sup>3</sup>, the density of the liquid is 0.96 g/ml<sup>3</sup>, the molecular viscosity of air is  $1.81 \times 10^{-4}$  cm<sup>2</sup>/sec, and gravity is 980.665 cm/sec<sup>2</sup>. Three different viscous fluids were tested in Kim et al.'s experiments, with viscosities 80, 200, and 600 Poise, respectively. Four airflow rates 330, 500, 830, and 1170 ml/sec, and two liquid feed rates 0.5 and 1 ml/min were used.

A comparison of the experimental measurement of the mean liquid thickness with the Poiseuille solutions is shown in figure 2(a). The data show that for each fluid tested the mean liquid thickness decays as the airflow rate increases, and the Poiseuille solutions do capture this trend, while grossly over-estimating the liquid layer thickness.

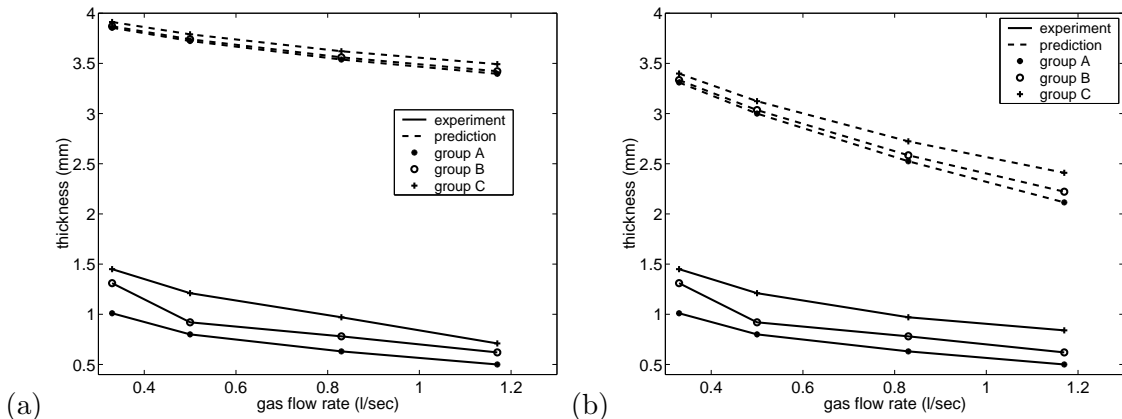


Figure 2: (a) Comparison of the Poiseuille solution with experimental data, where the liquid feed rate of the liquid is 0.5 ml/min. (b) The same as (a), but using effective viscosity.

## 1.2 Effective viscosity

To explain the discrepancy between the experimental measurement and the theoretical prediction, we estimate the Reynolds numbers for pipe flows in the experiments. Using

$$Re_D \equiv U_{ave} D / \nu,$$

where  $D$  is the diameter of the airway,  $U_{ave}$  is the cross-sectional average of the air velocity, and  $\nu$  is the kinematic viscosity, the (fast) airflow rate of 1170 ml/s yields for Reynolds number  $Re_D \approx (1170 \times 0.8) / (\pi \times (0.4)^2 \times 0.15) \approx 12500$ , while for an airflow rate of 330 ml/sec (slowest in the experiment) the Reynolds number is  $Re_D \approx 3500$ . It is known that for monophasic pipe flows the flow is said to be undergoing transition to turbulence at  $Re_D \approx 2000$ . Above  $Re_D \approx 3000$ , the pipe flow is fully turbulent [7] (page 117). Hence we expect the core airflow to be turbulent.

Suppose that the liquid is laminar, and the core is fully turbulent with no entrained droplets, the molecular viscosity of the gas can be replaced by an effective (eddy) viscosity  $\mu_{eff} = \mu_{T,G}$ , where  $\mu_{T,G}$  is the turbulent viscosity of the gas flow. In evaluating  $\mu_{T,G}$ , a conservative estimate of eddy viscosity for pipe flows can be derived from Blasius formula, neglecting any influence of rough or wavy surface [7] (pp 422)

$$\mu_{T,G} \cong 0.0791 \frac{(Re_D)^{3/4} \mu}{16}, \quad (7)$$

where  $\mu$  is molecular viscosity of gas, and  $Re_D$  is the Reynolds number defined above. After replacing the molecular viscosity by the effective viscosity in the Poiseuille solutions, we compare the experimental data with the resulting predictions. Figure 2(b) shows that the predictions using this effective viscosity formula (7) are an improvement with respect to those

from the exact Poiseuille solution, at least quantitatively. However, the predictions no longer capture the qualitative trend of the decay rate in liquid thickness for increasing gas flow rate. Notice that we estimated the effective viscosity based on the assumption that the core airflow is turbulent. The estimate is less conservative when the airflow rate is high, which brings the prediction closer to the experimental data than those of low airflow rates. This results in steeper slopes than those using the exact Poiseuille solution. We remark that the turbulence closure we used here is the so-called zero-equation model [7], whereby the molecular viscosity is simply replaced by an effective viscosity in the Poiseuille solution.

## 2 A two-phase gas-liquid model

Surface tension has long been known to play an important destabilizing role for two-phase liquid layer flows in cylindrical geometries, and the instability is responsible for wave generation [2, 4]. The theoretical prediction by means of Poiseuille solutions in the previous section neglects surface tension. Thus, these solutions fall short in two ways: (i) the predicted liquid layer is too thick, which implies that the liquid transport rate is lower than that of the experiment, and (ii) the  $z$ -independent interface does not agree with the undistorted smooth ring-shape waves observed in the experiment [5]. To investigate the role of surface tension effects in the rate of liquid transport, we derive a nonlinear evolution equation for the liquid thickness, based on lubrication or long-wave approximation. The derivation is similar to that in [6], but carried out here in cylindrical coordinates.

### 2.1 The evolution equation for a bounded film

Consider a viscous-liquid flow lining the inner wall of a vertical circular pipe, surrounding a pressure-driven gas flow. The side-views of the concentric two-phase pipe flow is shown in Figure 1(b). The governing equations for the liquid film are the incompressible axisymmetric Navier-Stokes equations in cylindrical coordinates (1). Equations (1) need to be nondimensionalized with respect to a set of scales. The length scale in the  $z$  direction is set by a typical wavelength  $\lambda$ , while the scale in the radial direction is  $R_1$ , the typical radius of the cross section of gas-column. The distortions is said to be of long-wave scale if  $\epsilon = R_1/\lambda \ll 1$ . Other scales are set by an axial velocity  $U_0$  and a radial velocity  $W_0$ . Continuity equation requires  $W_0 = \epsilon U_0$ . The list of all dimensionless variables is as follows:

$$\begin{aligned} r^* &= r/R_1, \quad z^* = z/\lambda, \quad u^* = u/U_0, \quad w^* = w/W_0, \\ t^* &= t U_0/\lambda, \quad p^* = \epsilon p R_1/(\mu^{(l)} U_0), \quad \tau^* = \tau R_1/(\mu^{(l)} U_0), \end{aligned} \tag{8}$$

where  $t^*$  is the dimensionless time,  $\tau^*$  is the dimensionless stress, and  $p^*$  is the dimensionless pressure. If the dimensionless variables are substituted into the system (1) and gravity is ab-

sorbed in the pressure term, then a scaled system for the liquid is (drop stars for dimensionless variables hereafter):

$$\begin{aligned}\epsilon Re^{(l)}(u_t + u u_z + w u_r) &= -p_z + \frac{1}{r} \partial_r(r u_r) + \epsilon^2 u_{zz} \\ \epsilon^3 Re^{(l)}(w_t + u w_z + w w_r) &= -p_r + \epsilon^2 \left( \frac{1}{r} \partial_r(r w_r) + \epsilon^2 w_{zz} - w/r^2 \right) \\ \frac{1}{r} \partial_r(r w) + u_z &= 0,\end{aligned}\tag{9}$$

with Reynolds number  $Re^{(l)} \equiv U_0 R_1/\nu^{(l)}$ . Boundary conditions are

$$u = 0, \quad w = 0,\tag{10}$$

at the inner wall of the pipe,  $r = a$ . Assuming that the surface tension of the liquid is constant in  $z$ , the conditions at the interface,  $r = R$ , are (i) continuity of tangential stress

$$(u_r + \epsilon^2 w_z)(1 - \epsilon^2 R_z) + 2\epsilon^2(w_r - u_z) = \tau^{(g)}(1 + (\epsilon R_z)^2),\tag{11}$$

where  $\tau^{(g)}$  is the dimensionless tangential stress of gas, and (ii) jump of normal component of stress is given by Laplace's formula

$$\begin{aligned}-p(1 + (\epsilon R_z^2)) + 2\epsilon^2(w_r + u_z(\epsilon R_z)^2) + \epsilon^2(u_r + \epsilon w_z)R_z \\ = \left[ \pi^{(g)} + \epsilon C^{-1} \left( \frac{1}{R(1 + (\epsilon R_z)^2)^{1/2}} - \frac{\epsilon^2 R_{zz}}{(1 + (\epsilon R_z)^2)^{3/2}} \right) \right] (1 + (\epsilon R_z)^2),\end{aligned}\tag{12}$$

where  $\pi^{(g)}$  is the dimensionless normal stress of gas, and  $C = U_0\mu^{(l)}/\gamma$  is the capillary number [6].

Finally, the dimensionless kinematic condition at the interface is

$$w = R_t + u R_z.\tag{13}$$

Integrating the continuity equation across the annular-sectional area of the liquid and using (13) yields the layer-mean equation

$$R_t - \frac{1}{R} \frac{\partial}{\partial z} \int_R^a u r dr = 0\tag{14}$$

for the interface location. With an approximate solution for  $u$ , the system can be closed and reduced to a single evolution equation for the interface location.

The leading order approximation of  $u$  can be obtained by taking the limit  $\epsilon \rightarrow 0$  in equations (9)–(12). Since the liquid is highly viscous,  $Re^{(l)}$  is at most  $O(1)$  and hence  $\epsilon Re^{(l)} \rightarrow 0$ . While the higher-order terms vanish in the system of equations, similar to the planar case in [6], it is essential to retain the surface tension terms at the leading order, for which one term is of  $O(\epsilon)$ , and the other is of  $O(\epsilon^3)$ . The  $O(\epsilon)$  term is responsible to the onset of instability of

an initial disturbance, while the  $O(\epsilon^3)$ -term stabilizes the evolution. Hence it is important to retain both of them, regardless of the order of magnitude. A more careful asymptotic analysis would be required to justify this, however it will not be pursued here. It is also worth pointing out that because of the geometry, surface tension in the planar case consists of only the  $O(\epsilon^3)$  term. The long-wave regime in the planar case [6] does not have any instability.

At leading order in  $\epsilon$ , the momentum and continuity equations, in dimensional form, become

$$\mu^{(l)} \left( \frac{1}{r} \partial_r (r u_r) \right) = p_z^{(l)}, \quad (15)$$

$$0 = p_r^{(l)}, \quad (16)$$

$$R_t - \frac{1}{R} \frac{\partial}{\partial z} \int_R^a u r dr = 0. \quad (17)$$

The boundary condition at  $r = a$  is

$$u = 0. \quad (18)$$

At the interface  $r = R$  we have

$$\mu^{(l)} u_r = \tau^{(g)}, \quad (19)$$

$$-p^{(l)} = -p^{(g)} + \gamma(R^{-1} - R_{zz}). \quad (20)$$

From equations (15), (16), (18)–(20), the boundary value problem has a solution of the form

$$u(r) = \frac{p_z^{(l)}}{4\mu^{(l)}} (r^2 - a^2) + A \ln(r/a), \quad (21)$$

where  $A = R(\tau^{(g)} - 1/2 p_z^{(l)} R)$ . From (20),  $p_z^{(l)}$  is known through  $p_z^{(g)}$ , hence the terms that need to be determined in formula (21) are  $p_z^{(g)}$  and  $\tau^{(g)}$ , the  $z$ -component of the pressure gradient and the shear stress from the gas flow.

To model the gas flow, we adopt the so-called zero equation turbulence closure [7]. We proceed to compute the mean flow using again a Poiseuille solution, modulated to take into account the slow variation in  $z$  of the gas-liquid interface. More refined closure models can certainly be used, especially taking into account the wavy surface, but we leave this study to future work. The solution  $u$  for Poiseuille flow is of the form

$$u(r) = \frac{p_z}{4\mu} r^2 + c(z). \quad (22)$$

We need a boundary (interfacial) condition to determine  $c(z)$ . Since the dynamic viscosity ratio of liquid to gas is of order  $10^6$ , by continuity of velocity, it may be appropriate to assume that the velocity at the interface  $r = R(z, t)$ , is of order  $\epsilon$  or smaller. Hence we assume for the mean velocity field of the gas

$$u^{(g)}(r) = \frac{p_z^{(g)}}{4\mu^{(g)}} (r^2 - R^2). \quad (23)$$

With this velocity, the flux function for gas is

$$Q^{(g)}(z) = \int_0^{R(z)} u^{(g)} 2\pi r dr = -\frac{\pi p_z^{(g)} R(z)^4}{8\mu^{(g)}}. \quad (24)$$

If the flux,  $Q^{(g)}$ , is kept constant, the  $z$ -component of the gas pressure gradient is

$$p_z^{(g)}(z) = -\frac{8Q^{(g)}\mu^{(g)}}{\pi R(z)^4}. \quad (25)$$

Similarly, the tangential stress at the interface is

$$\begin{aligned} \tau^{(g)}(z) &= \mu^{(g)} u_r^{(g)}|_{r=R(z)} \\ &= -\frac{4Q^{(g)}\mu^{(g)}}{\pi R(z)^3}. \end{aligned} \quad (26)$$

Substituting these two terms, (25) and (26), into (21) results in the approximation for the liquid velocity field. The velocity field is then put into the continuity equation (14) to obtain the nonlinear evolution equation for the interface location  $R$ . The dimensional evolution equation can finally be written as:

$$\begin{aligned} \mu^{(l)} R_t + \frac{2a^2 Q^{(g)} \mu^{(g)}}{\pi R^4} \left[ \left( \frac{a}{R} \right)^2 - 1 \right] R_z - \frac{\gamma}{8} \left[ \left( \frac{a}{R} \right)^4 - 1 + 4 \ln(R/a) \right] R_z^2 \\ - \frac{\gamma}{16} \left[ -\frac{a^4}{R^3} + \frac{4a^2}{R} - 3R + 4R \ln(r/a) \right] R_{zz} \\ - \frac{\gamma}{2} \left[ a^2 - R^2 + 2R^2 \ln(R/a) \right] R_{zzz} R_z \\ - \frac{\gamma}{16} \left[ -\frac{a^4}{R} + 4a^2 R - 3R^3 + 4R^3 \ln(R/a) \right] R_{zzzz} = 0. \end{aligned} \quad (27)$$

Normal-mode analysis can be applied to the above equation to investigate the behavior of small perturbations of a uniform film  $r = R_0$ . In particular, the behavior reflecting how (small) wavenumbers surface tension parameter, and mean radius  $R_0$ , are related to instability growth can be analyzed.

The experiment with which we compare the mean thickness of the liquid layer was conducted with a given fixed liquid feed rate. This implies that the mean liquid flux in our model must be kept constant. The flux function at any point  $z$  and time  $t$  is given by

$$\begin{aligned} \mu^{(l)} Q^{(l)} &= \mu^{(g)} Q^{(g)} \left[ \left( \frac{a}{R} \right)^2 - 1 \right]^2 \\ &+ \frac{\pi\gamma}{8} \left[ -\frac{a^4}{R^2} + 4a^2 - 3R^2 + 4R^2 \ln(R/a) \right] R_z \\ &+ \frac{\pi\gamma}{8} R^2 \left[ -\frac{a^4}{R^2} + 4a^2 - 3R^2 + 4R^2 \ln(R/a) \right] R_{zzz}. \end{aligned} \quad (28)$$

It is worth pointing out that equation (27) does not make an assumption of a small ratio of liquid thickness to pipe radius. Although this assumption makes a number of simplifying

approximations possible, in particular to promote the surface tension effect to be of the same order as pressure, it might not be suitable for our problem. For instance, in [2], the ratio of liquid thickness to pipe radius must be assumed of order  $\beta \approx 10^{-2}$  or smaller, unless the radius is fairly small, e.g.  $10^{-3}$  cm or smaller. For our problem the radius of pipe is 0.5 cm, and the mean liquid thickness ranges from 0.05 cm to 0.1 cm for different gas flow rates, provided the mean liquid flux is 0.5 ml/min.

For the initial-boundary-value problem (27), the boundary conditions have to be determined from those of the experiment under the same scaling and approximations that went into deriving the model. It is not clear how to pursue this, but convenient choice suitable for conditions away from the ends of (sufficiently long) pipes is offered by periodic boundary conditions. In the next section, we solve numerically this evolution equation with periodic boundary conditions, while maintaining a fixed mean liquid flux as required by the experiment. The resulting mean thickness of the liquid is our theoretical prediction.

## 2.2 Numerical solutions and comparison

Equation (27) is solved by the standard *method of lines*: first, spatial derivatives are discretized with the second-order center differencing, generating a system of coupled ordinary differential equations (ODE) in time for the variable  $R$ , then the ODE is solved by an ODE solver. Due to high spatial derivatives in the equation, time-step restriction to the resulting ODE is severe, and it is necessary to employ an implicit time-stepping method for the solution. Gear’s method as implemented in the ODE solver DLSODE from Netlib is used for solving our system of ODE, and has proved to be efficient and stable. Since equation (27) is solved with periodic boundary conditions, we look at the initial condition of the form

$$R(0, z) = R_0 - \beta \cos \frac{2\pi z}{L}, \quad (29)$$

where  $L$  is the period, and the periodical domain is a multiple of  $L$ .

The surface tension value of the liquid is required for solving equation (27). Since the values of the silicone oils used in the experiment are not documented, we choose the values suggested by [3], page 147: the surface tension values for silicone oils whose viscosities range from 4.86 to 122 Poise vary from 21.1 to 21.5 dyn/cm. The density of the silicone oil listed in [3] is 0.971–0.975 g/cm<sup>3</sup> which is comparable to that of the experiment. The viscosity values of the silicone oils in the experiment are 80, 200, 600 Poise, respectively. Extrapolating linearly, we use the values 21.4, 21.75, and 22 dyn/cm for our calculations.

The experiment was conducted with a fixed gas flow rate and a fixed liquid feed rate. The fixed gas flow is incorporated into the model, but the fixed liquid feed rate is not satisfied automatically with periodic boundary conditions. Our strategy is to choose an initial mean height perturbed by a small-amplitude periodical wave as shown in equation (29). We run the

code and monitor the liquid flux computed by formula (28), until the flux reaches a “quasi-steady” value consistent with that of the experiment. Then the averaged mean thickness over a time period is used as our theoretical prediction.

Figure 3 (a) is a plot of theoretical predictions against experimental data using the model described in this section. The periodical domain is  $2\pi$ , and the effective viscosity (7) is used in the calculation. We see the trend of the experiment is captured by the model, except for group B with flow rates between 330 and 500 ml/sec.

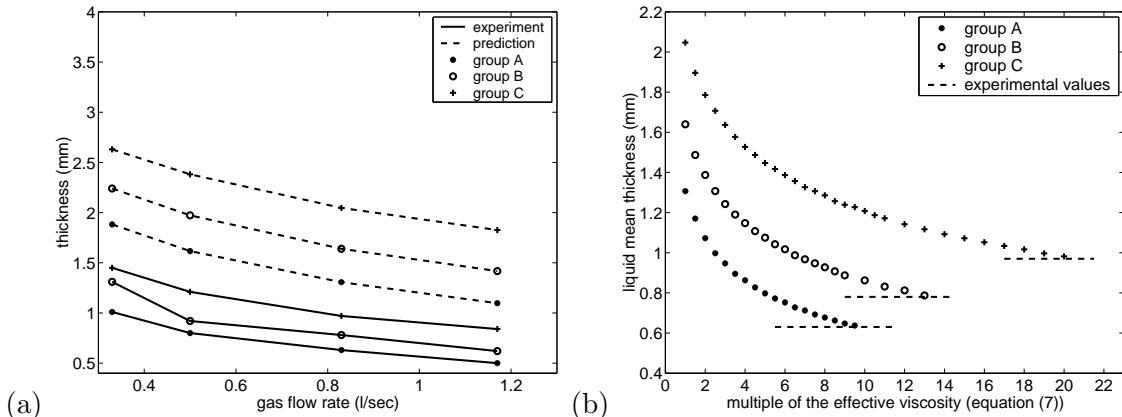


Figure 3: (a) The comparison of the predicted liquid mean thickness with the experimental data. (b) Projected viscosity values for predicted mean thicknesses to match the experimental data. The gas flow rate is 830 ml/sec.

### 2.3 Modified effective viscosity

The effective viscosity (7) is derived from the Blasius formula for smooth-wall data of monophasic pipe flows. It is likely to be a conservative estimate for wavy surfaces, just as it is for rough surfaces. To modify the effective viscosity for our problem, we perform a sequence of simulations for one particular gas flow rate, with different effective viscosities, in the unit of  $\mu_{T,G}$  defined in (7), until our predictions match experimental data. Figure 4(a) shows the projected viscosity values for predicted mean thicknesses to match the experimental data. The gas flow rate is 830 ml/sec. By examining these values, we notice that the effective gas viscosity that matches the experiments may depend on the liquid viscosities. We hence propose a modified effective viscosity for our problem

$$\mu_{\text{eff}} \cong (m^{1/5}) 0.0791 \frac{(Re_D)^{3/4} \mu}{16}, \quad (30)$$

where  $m = \mu^{(l)}/\mu^{(g)}$ , the ratio of liquid viscosity  $\mu^{(l)}$  to the molecular viscosity of gas  $\mu^{(g)}$ . The power law of  $m$  approximates the projected values shown in Figure 3(b), namely the associated

$x$ -coordinate when each curve touches the horizontal dash line.

Using this modified effective viscosity, we repeat the simulations for predicting the mean liquid thickness. Figure 4 shows the predictions match the experimental data. The liquid feed rate is 0.5 ml/min in (a) and 1 ml/min in (b). The mean liquid flux in the simulation is kept at  $0.5 \pm 0.005$  ml/min in Figure 4(a) and  $1.0 \pm 0.005$  ml/min in (b).

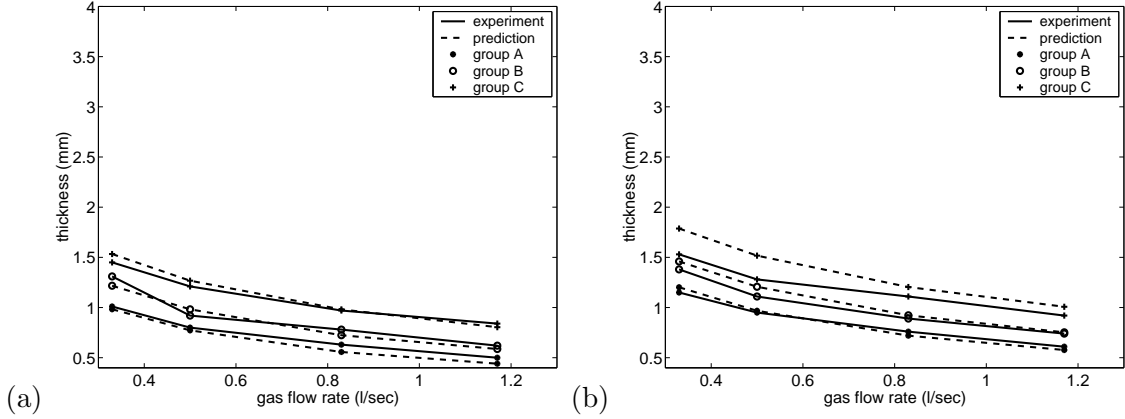


Figure 4: (a) A comparison of predicted mean liquid thickness with the experiment using the wave model and the modified effective viscosity. The liquid feed rate is 0.5 ml/min. (b) The same as (a) but with double liquid feed rate 1 ml/min

## 2.4 Surface tension parameter

If the power-law modification for the effective viscosity is not used in our calculations, the predicted mean liquid thicknesses are thicker than those reported in the experiment, as shown in Figure 3(a). To investigate the discrepancy, we plot the waveforms of the interfacial waves. Figure 5(a) shows snap shots of the interfacial waves that develops from the initial perturbation after a sufficiently long time has elapsed to saturate the initial instability. At time  $t = 168$ , wave snapshots are shown for each of the three groups, with liquid viscosity, from the top, of 80, 200, and 600 Poise respectively. The effective viscosity without the power-law modification is used for the calculation. The gas flow rate is 330 ml/sec. For all three groups, the wavelength is about 30 mm, the mean height is less than 2.7 mm, and the amplitude is less than 0.2 mm. It is clear that the waves are within the long-wave regime, whereas the wave amplitudes are small compared with the layer means. A remedy for the thickness discrepancy can be offered by large amplitude waves. These waves could provide the additional liquid flux needed for the model, and the key for generating large amplitude waves is larger surface tension values.

The paper by Bechtel et al. [1] suggests that for certain fluids a dynamic surface tension, in contrast to the static surface tension measured under equilibrium conditions, needs to be taken

into account. It remains to be seen whether silicon oils of the kind used in the experiment are fluids for which this quantity plays a role, but the wavy motion in the experiment might belong to the class of flows where dynamic surface tension appears. As a preliminary attempt to investigate this dynamic effect and to parametrize it, we collect the different values of constant surface tensions needed to match the experimental data by performing a sequence of computations.

Figure 5(b) shows the interfacial dynamics for liquid with viscosity 80, 200, and 600 Poises respectively. The surface tension values are chosen to be 390, 400, and 600. These values are the ones for which the mean liquid fluxes are  $0.5 \pm 0.01$  ml/min after waves are saturated and propagate in and out of the periodic domain several times, while the mean liquid thicknesses match the experimental values. The gas flow in the calculation is 330 ml/sec and the effective viscosity without power-law modification is used. We see that, from the initial axisymmetric perturbation of the interface, large amplitude waves evolve and saturate into a wave-train propagating to the right. These waves are consistent with observation of undistorted smooth ring-shape waves reported in the paper of Kim et al. [5].

A more thorough study is necessary for us to characterize the surface tension effect in this problem. Nonetheless, the evolution equation derived in this paper might be used as a model to measure the dynamic surface tension in the experimental data of these highly viscous liquid in two-phase pipe flows.

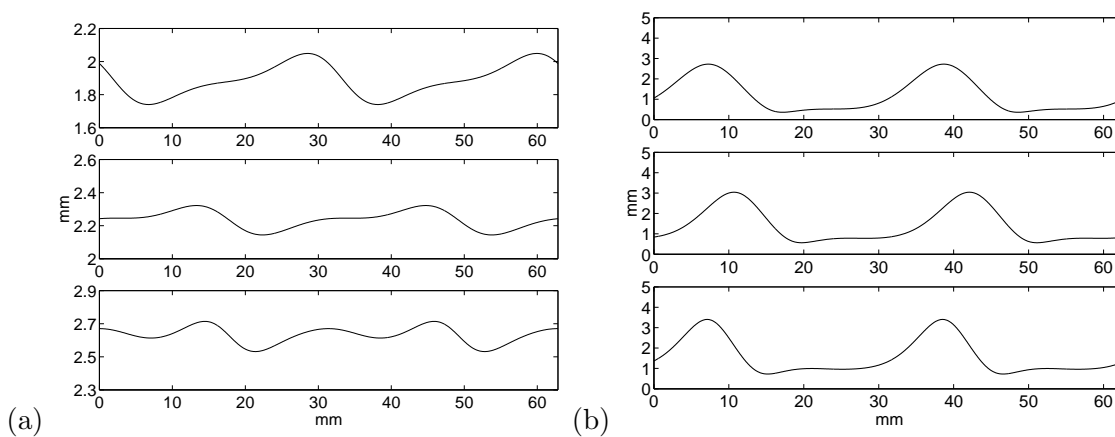


Figure 5: (a) Interface dynamics at  $t = 168$ . From the top, the liquid viscosity is 80, 200, and 600 Poise respectively. The effective viscosity without power-law modification is used. The gas flow rate is 330 ml/sec. (b) Same as (a), but with surface tension values chosen so that the predicted mean thicknesses match the experimental data.

### 3 Discussion and conclusion

We have presented several models for predicting the mean liquid thickness in the experiment by Kim et al. [5]. The models do capture the main behavior of the newtonian liquids reported in this reference. With the help of a modified effective viscosity, fitted on just one datum for each fluid group, the model evolution equation is able to predict with some quantitative agreement the experimental data. Nevertheless the model, to some extent, fares worse with respect to the data relative to the largest viscosity fluid, and this mismatch worsen for the fastest liquid feed rate 1 ml/min.

Improving the agreement and prediction capability of the model should be achievable by modelling more accurately the stress at the interface beyond the zero-equation turbulence model. In fact, the lack of sufficiently strong tangential stress at the interface results in weaker momentum transfer from the gas to the liquid, and hence in a reduced liquid transport rate. Thus, a thinner liquid layer cannot support a fixed liquid feed. Increasing momentum transfer requires either a larger surface tension, which increases the pressure contribution to this transfer, and/or an effective viscosity for the gas that increases the tangential stress contribution. A model similar to the wind-over-waves coupling for pipe flows could generate enhanced wave-induced shear stress, with turbulent gas flow over non-breaking waves. Whether this approach can make up for the inadequate momentum transfer at the interface remains to be seen and is under investigation.

Treating surface tension as a parameter offers an alternative to the route of modified effective viscosity. In this respect, we notice that dynamical (as opposed to static) surface tension variation by order of magnitudes have been reported in the literature for certain liquid mixtures. The applicability to the present experiment is another direction of investigation we are currently pursuing.

### References

- [1] S. E. Bechtel, J. A. Cooper, M. G. Forest, N. A. Petersson, D. L. Reichard, A. Saleh, and V. Venkataramanan. A new model to determine dynamic surface tension and elongational viscosity using oscillating jet measurements *J. Fluid Mech.*, 293:379-403, 1995
- [2] P. S. Hammond. Nonlinear adjustment of a thin annular film of viscous fluid surrounding a thread of another within a circular cylindrical pipe *J. Fluid Mech.*, 137:363-384, 1983.
- [3] D. D. Joseph and Y. Y. Renardy. *Fundamentals of two-fluid dynamics: part I: mathematical theory and applications* Springer-Verlag, 1992.

- [4] V. Kerchman. Strongly nonlinear interfacial dynamics in core-annular flows *J. Fluid Mech.*, 290:131-166, 1995.
- [5] C. S. Kim, M. A. Greene, S. Sankaran, and M. A. Sackner. Mucus transport in the airway by two-phase gas-liquid flow mechanism - continuous-flow model *Journal of Applied Physiology*, 60:908-917, 1986.
- [6] A. Oron, S. H. Davis, and S. G. Bankoff. Long-scale evolution of thin liquid films *Reviews of Modern Physics*, 69:931-980, 1997.
- [7] F. M. White. *Viscous Fluid Flow* 2nd edition, McGraw-Hill, New York, 1991.